ISSN 0027-1349, Moscow University Physics Bulletin, 2016, Vol. 71, No. 1, pp. 105–113. © Allerton Press, Inc., 2016.

CONDENSED MATTER PHYSICS

The Characteristic Investigation of Spray Coated W Incorporated in Oxide Thin Films[1]

G. Turgut[a] and E. F. Keskenler[b]

[a] Erzurum Technical University, Science Faculty, Department of Basic Sciences, 25240 Erzurum, Turkey

[b] RecepTayyip Erdogan University, Faculty of Engineering, Department of Nanotechnology, 53100 Rize, Turkey

e-mail: guventrgt@gmail.com, guven.turgut@erzurum.edu.tr

Received May 20, 2015

Abstract—W incorporated tin oxide (TO) thin films were grown via spray pyrolysis with various tungsten contents. The films were observed to be polycrystalline tetragonal crystal nature with (301) and (211) preferential planes. From EDX analysis, it was seen the tungsten concentrations in the TO films were slightly higher than ones in the starting solutions. Polyhedron-like and small rod like grains were observed in the SEM images. 3 at % W doped tin oxide film has minimum sheet resistance (44.67 Ohm) and resistivity (3.685×10^{-3} Ohm cm) values and maximum figure of merit (75.74×10^{-5} Ohm^{-1}) value. The optical band gap (E_g) of pure film raised from 3.84 to 3.91 eV with 3 at % W contribution level.

Keywords: tin oxide, W doping, spray pyrolysis, thin films

DOI: 10.3103/S0027134915030108

1. INTRODUCTION

Transparent conducting oxides (TCOs) have gained a great attention due to their unique features [1, 2]. The stoichiometric tin oxide, which is a member of TCO family, is an insulator but non-stoichiometry, in particular oxygen deficiency, gives rise to an increase in its conductivity [3, 4]. TO with wide-band gap semiconductor property [5] is wide-spread utilized in a variety of technological devices such as solar windows, gas sensors, digital displays, touch-sensitive switches and architectural windows [2, 6–8], etc. because of its excellent electrical and optical characteristics, chemical and mechanical stability [9]. Further, TO thin films are stable up to high temperatures, excellent resistant to strong acids and very good adhesive to many substrates [10–12].

The certain features of TO materials may be healed by contribution atoms such as fluorine (F), antimony (Sb), neodymium (Nd), vanadium (V), and tungsten (W) etc. The W has various oxidation states until W^{6+}, and the radius of W^{6+} is the closer to that of Sn^{4+} (W^{6+}: 67 pm, Sn^{4+}: 71 pm) [13]. This causes an easy replacement of W^{6+} by Sn^{4+} ions. It is expected an increase in the electrical conductivity and optical transparency of degenerate TO semiconductor thin films with tungsten doping, since W introduces to generate a sufficient number of carriers in TO by replacing W^{6+} and Sn^{4+} ions.

In the earlier studies, many research groups have fabricated WTO thin films by using the sol-gel technique [14], pulsed plasma deposition (PPD) [13, 15, 16] pulsed laser deposition (PLD) [17], reactive evaporation [18]. As well as these techniques, another deposition technique is spray pyrolysis. The spray pyrolysis technique is very useful to deposit thin film materials because of its easy and cheap apparatus [19], easy doping of materials, capabilities of wide field coating and mass production [20]. According to our best knowledge, W doped TO samples have not been prepared via spray pyrolysis method. Thus, we have prepared W doped TO thin films for the first time by spray pyrolysis and we investigated that W doping effect on the structural, morphological, optical and electrical properties of TO.

2. EXPERIMENTAL

The pure and W doped tin oxide (WTO) thin films, reported in the present study, were prepared using a homemade spray pyrolysis experimental apparatus. Spray solutions prepared with stannous chloride dehydrate ($SnCl_2 \cdot 2H_2O$), tungsten hexachloride (WCl_6), isopropyl alcohol (C_3H_8O) as starting material, dopant source, and solvent, respectively. Moholkar et al. [21, 22] have investigated the solvent effect on some properties of spray deposited fluorine doped TO thin films and they found that isopropyl alcohol were the best solvent for these films. For this reasons, we used isopropyl alcohol as solvent for undoped and WTO

[1] The article is published in the original.

Table 1. Standard and observed "d" values of WTO thin films

(*hkl*)	Standard d (Å)	Calculated d (Å)					
		Undoped SnO_2	1 at % W doped SnO_2	2 at % W doped SnO_2	3 at % W doped SnO_2	4 at % W doped SnO_2	5 at % W doped SnO_2
110	3.3470	3.3664	3.3504	3.3495	3.3417	3.3593	3.3651
101	2.6427	2.6559	2.6468	2.6450	2.6410	2.6511	2.6577
200	2.3690	2.3768	2.3663	2.3712	2.3773	2.3768	2.3765
211	1.7641	1.7696	1.7651	1.7664	1.7669	1.7689	1.7695
220	1.6750	1.6787	1.6741	1.6740	1.6749	1.6773	1.3762
310	1.4984	1.4919	1.4941	1.5019	1.5020	1.5015	1.5013
301	1.4155	1.4195	1.4165	1.4176	1.4179	1.4181	1.4192
321	1.2147	1.2177	1.2162	1.2162	1.2167	1.2171	1.2162

thin films. 0.7 M stannous chloride dehydrate and 0.7 M tungsten hexachloride, precursor and dopant solutions, respectively, were mixed in different atomic ratios altered from 0 to 5 at % with step of 1 at %. A few drops hydrochloric acid (HCl) was added to six different solutions to increase resolution of stannous chloride and tungsten hexachloride. We used ordinary glass as substrate, which they cleaned with boiling chromic acid solution, acetone, deionized water and methanol. The substrates were warmed to the necessary temperature of 500°C. The constant experimental parameters are nozzle-substrate distance (40 cm), the flux rate (2.5 ml/min.) of filtered air and amount of solution (25 ml). The total deposition time was 10 minutes for each film. After deposition, the coated substrates were allowed to cool down naturally to room temperature. In each process, more five samples were produced simultaneously at each doping levels.

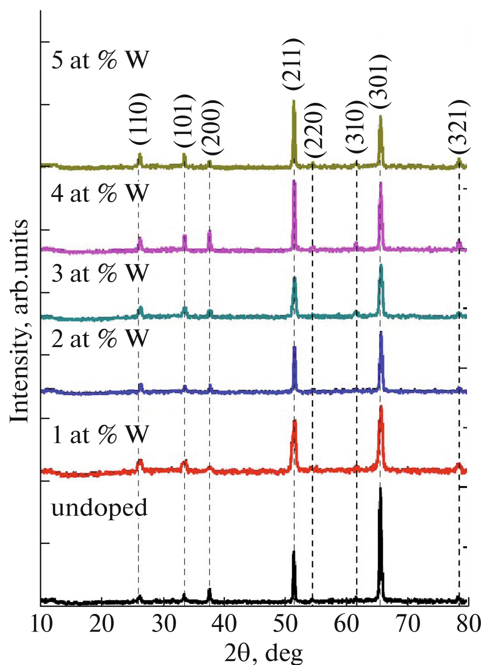

Fig. 1. XRD patterns of WTO thin films.

The crystalline investigation of the W doped SnO_2 samples was made by a RigakuMiniflex II X-ray diffractometer (XRD) with CuK_α radiation (λ = 1.5418 Å). For diffraction measurement at the room temperature, the values of 2θ were changed from 10° to 80°. The topographic features and element composition for pure and W doped films were investigated by scanning electron microscope (SEM-LEO 440) and energy dispersive x-ray (EDX) measurements. The sheet resistance measurements for WTO samples were done with four point probe. The optical transmittance were recorded in spectral region of 300–1000 nm by means of UV-VIS spectrometer (Perkin-Elmer, Lambda 40) which works in the range of 200–1100 nm.

3. RESULTS AND DISCUSSIONS

3.1. Crystalline Features

The crystalline features of WTO samples was inquired by XRD patterns. Figure 1 shows XRD spectra of pure and W incorporated tin oxide samples. This spectra indicates that pure and W doped TO have (110), (101), (200), (211), (220), (310), (301) and (321) planes. Any peak belonging to tungsten is not detected. Undoped, 1, 2 and 3 at % W doped TO samples have the strongest (301) plane, but it slightly changes to (211) preferential orientation for 4 and 5 at % W contribution levels. For 4 and 5 at % W doping ratios, the (301) and (211) peaks are comparable, but (211) peak intensity is stronger than one of (301). The (301) preferential orientation of undoped film has been observed by Elangovan et al. [19] and the (211) preferential orientation for undoped/doped films has been observed by Babar et al. [23]. In studies made by Smith et al. [24], Morris and McElnea [25], it was

Table 2. The structural properties of W doped TO films

Sample	W/Sn ratio	Lattice constants, Å		Grain Size (D nm)	Microstrain ($\varepsilon \times 10^{-5}$)	Dislocation density ($\delta \times 10^{12}$ lines/m^2)
		a	c			
Undoped SnO_2	0	4.7608	3.2001	194.25 (38.90–(211))	13.079	26.502
1 at % W doped SnO_2	1.06	4.7382	3.1911	282.44 (26.47–(211))	8.034	12.536
2 at % W doped SnO_2	2.74	4.7369	3.1883	304.42 (18.62–(211))	5.102	10.791
3 at % W doped SnO_2	3.24	4.7259	3.1847	332.40 (34.92–(211))	4.664	9.051
4 at % W doped SnO_2	4.14	4.7508	3.1948	36.05 (205.09–(301))	68.172	769.300
5 at % W doped SnO_2	5.13	4.7590	3.2039	35.67 (192.63–(301))	69.685	786.020

found that the content of spray solutions effected preferred orientation of TO films. In present study, preferential orientation of the films may also be changed by W doping concentrations, because W doping ratio changes spray solution content. As seen in Fig. 1, the strongest (301) peak of undoped film firstly decreases with 1 at % W contribution. Further W doping ratio do not much change preferential peak intensity. The observed "d" values are presented in Table 1 and these values are compared with the standard ones from the JPCDS card no. 41-1445. The matching of the observed and standard "d" values suggests that the deposited films have tin oxide crystalline with cassite rite tetragonal structure. The lattice constants "a" and "c", for tetragonal phase structure is determined by relation [26];

$$\frac{1}{d^2} = \left(\frac{h^2 + k^2}{a^2}\right) + \left(\frac{l^2}{c^2}\right) \tag{1}$$

where "d" is the interplaner distance and (hkl) miller indices, respectively. The calculated and standard lattice constants are given in Table 2. The calculated "a" and "c" values agree with ones from JPCDS card no. 41-1445 ($a = b = 4.7382$ Å, $c = 3.1871$ Å). As seen from Table 2, the lattice constant values of undoped sample slightly decrease with W doping up to 3 at % ratio, then they go up with more W contribution level. For the most striking peaks of (301) and (211), the average grain size is calculated by using Scherrer formula [8],

$$D = \frac{0.9\lambda}{(\beta\cos\theta)} \tag{2}$$

where D is mean the grain size of nanoparticles, β is the full width at half of the peak maximum (FWHM) in radians and "θ" is Bragg's angle. As seen in Table 2 and Fig. 2, the calculated D value of 194.25 nm for pure TO sample increases to values of 282.44, 304.42 and 332. 40 nm for 1, 2 and 3 at % W doping levels, respectively. The calculated grain size values of (301) peak for 4 and 5 at % W doped films are 205.09 and 192.63 nm, respectively. These values are not intended to the most striking peak. D values of the most striking (211) peak for 4 and 5 at % W doped TO have been computed as 36.05 and 35.67 nm, respectively. Namely, average grain size significantly decreased with 4 and 5 at % W contribution ratios.

Misfit stress, which is one of the most significant effects, negatively impressed crystalline features. The geometric mismatches between film and substrate may introduce stress [27]. As known, stress gives rise to microstrains for films. The microstrain (ε) values of WTO films are calculated by relation [28];

$$\varepsilon = \left(\frac{1}{\sin\theta}\right)\left[\left(\frac{\lambda_x}{D}\right) - (\beta\cos\theta)\right] \tag{3}$$

The calculated ε values are given in Table 2. It is observed that the ε values exhibits a decreasing tendency with increasing W doping concentration up to 3 at %, and then an increasing tendency with further W content. This can be explained that the extra doping concentration, after 3 at %, increases the W ionic densities as defects in the interstitial of the crystal structures and the strain increases.

For the preferential orientations, the dislocation density(δ) for samples is estimated using the equation [6],

$$\delta = 1/D^2$$

Since δ is the measure of the amount of the defects in a crystal, the small value of δ obtained for 3 at % W

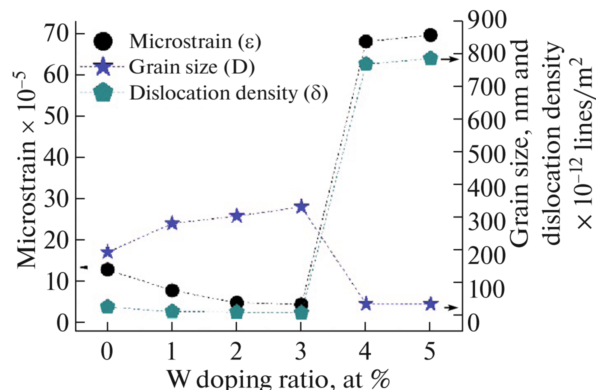

Fig. 2. The variation of grain size and dislocation density with W doping ratio.

Table 3. The electrical and optical properties of WTO films

Sample	R_s, Ω	ρ (×10^{-3} Ω cm)	Transmittance at 550 nm, %	E_g, eV	Φ (×10^{-5} $Ω^{-1}$)
Undoped SnO_2	91.85	7.578	59.93	3.84	7.89
1 at % W doped SnO_2	75.94	6.265	60.69	3.87	10.82
2 at % W doped SnO_2	48.08	3.967	67.16	3.89	47.06
3 at % W doped SnO_2	44.67	3.685	69.82	3.91	75.74
4 at % W doped SnO_2	52.12	4.307	57.27	3.79	8.81
5 at % W doped SnO_2	60.91	5.025	51.94	3.71	2.84

doped TO film confirms that 3 at % W content increased the crystallinity of TO.

3.2. Morphological Properties

The W/Sn atomic ratios in WTO thin films were determined by EDX measurement. EDX graphs for samples are given in Figs. 3a–3f. EDX image clearly indicates the presence tin and tungsten elements in the samples. The atomic ratios of W/(W + Sn) (at %) participated in the starting solution are lower slightly than ones in grown films (see Table 2). The average thickness of WTOs is about estimated to be 825 nm by cross-sectional SEM picture (Fig. 4a). The SEM images of WTO films are given in Fig. 4. It can be seen the distribution of the grains in the surfaces is uniform and the distribution of the grain, grain sizes and grain shapes depend on W doping ratios. The undoped film (Fig. 4b) have polyhedron-like grains. The bigger grains start appearing on the surface with W doping up to 3 at % (Figs. 4c, 4d, 4e). After 3 at % W doping ratio, the grain size shows a decreasing tendency with further increasing W ratio. The number of polyhedron-like grains decrease on the surface of 4 at % W doped film

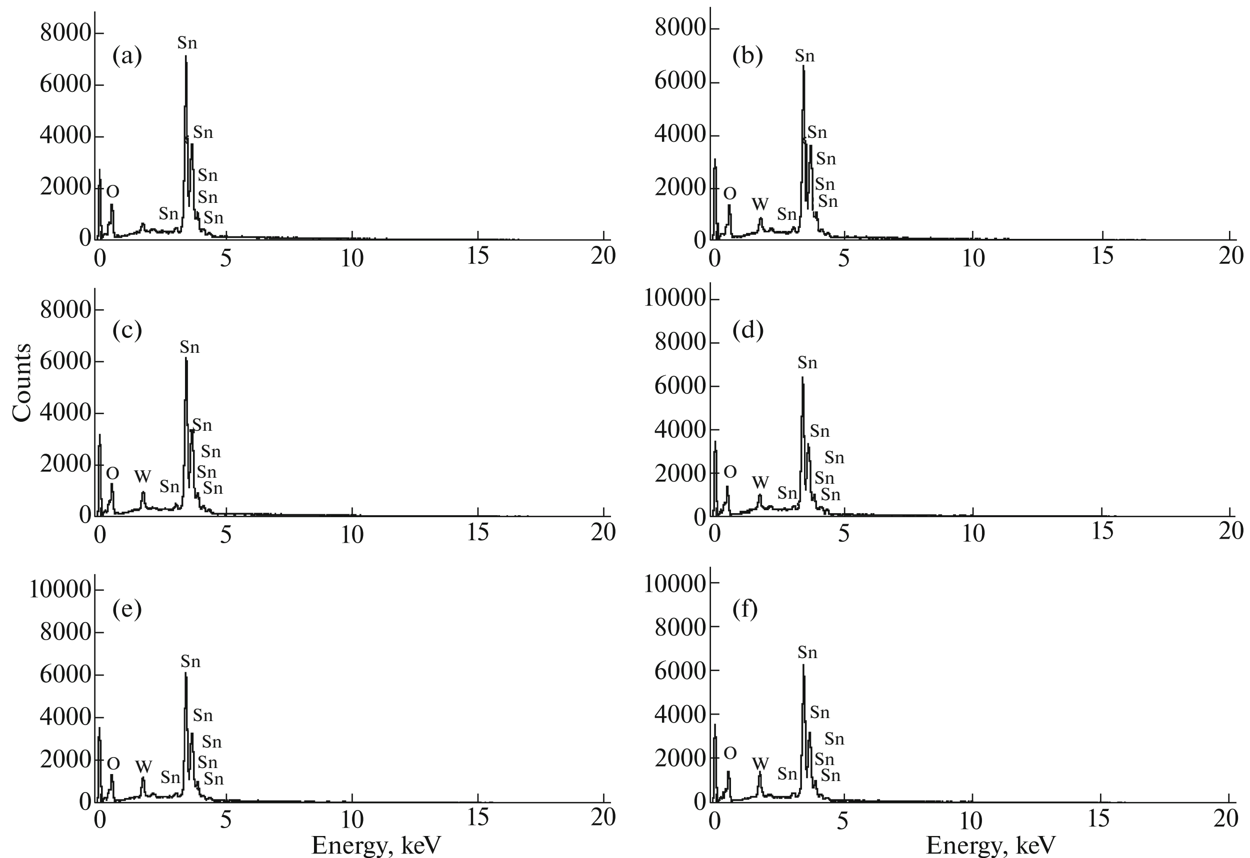

Fig. 3. EDX spectra of WTO films; (a) undoped (b) 1 at % W doped (c) 2 at % W doped (d) 3 at % W doped (e) 4 at % W doped (f) 5 at % W doped TO.

Table 4. A comparison of some electrical and optical properties of W doped SnO_2 films with studies in literature

Method/W doping level	Crystal structure	The lowest resistivity (Ω cm)	The lowest sheet resistance, Ω	The highest optical band gap, eV	Ref.
Sol-gel spin coating /2 at % for SnO_2	Cubic and tetragonal	/	7.11 × 103	4.115	[40]
Pulsed plasma deposition with post-annealing /3 wt % for SnO_2	Tetragonal rutile	6.84×10^{-4}	/	4.22	[13]
Sol–gel dip coating /3 at % for SnO_2	Tetragonal rutile	5.8×10^{-3}	/	/	[14]
Pulsed plasma deposition method with a post-annealing /3 wt % for SnO_2	Tetragonal rutile	6.67×10^{-4}	/	4.22	[15]
Pulsed plasma deposition /3 wt % for SnO_2	Tetragonal rutile	2.1×10^{-3}	/	4.02	[16]
Sol–gel dip coating /3 mol % for SnO_2		2.9×10^{-2}	/	/	[41]
Pulsed laser deposition /2 at. % for SnO_2 deposited on glass	Tetragonal rutile	7×10^{-4}/			
Pulsed laser deposition /1.5 at % for SnO_2 deposited on TiO_2 seed onto glass	Tetragonal rutile	3.5×10^{-4}	/	/	[17]
Reactive deposition /2 mol % for SnO_2	Rutile structure	$\sim 10^{-2}$	/	/	[18]
Spray Pyrolysis /2 at % for 20 at % F doped SnO_2	Tetragonal rutile	/	1.12	4.14	[42]
Spray Pyrolysis /3 at % for SnO_2	Tetragonal rutile	3.685×10^{-3}	44.67	3.91	**Present study**

and the smaller rod-like grains have started appearing. When doping ratio is 5 at %, the surface of the films has been almost covered with small sized rod-like grains. The same difference in orientation is reflected in SEM studies as they lead to different grain shapes. Also, SEM results collaborate with grain size and preferential orientation tendency with W doping ratio from XRD analysis. In addition, the familiar grain shapes were obtained by Babar et al. [29, 30], Ravichandran and Philominathan [31].

3.3. Electrical Properties

It was found that the films have n-type conduction by the hot probe technique. Electrical characterization for pure and W incorporated samples were done with four point probe method. Sheet resistance (R_s) and resistivity (ρ) values for samples are shown in Table 3 and their variation with W doping ratio are given in Fig. 5. The R_s and ρ values for samples change between 91.85 and 44.67 Ω, 7.578×10^{-3} and 3.685×10^{-3} Ω cm, respectively. In Fig. 5, there is a decrement in R_s and ρ values of pure film up to 3 at % W doping level, then R_s and ρ values raise with more W contribution level irrespective of doping levels. The resistivity values obtained in this study are on the order of 10^{-3} Ω cm and are one order of magnitude higher than those reported in some studies by Huan et al. [13, 15], but they have the same order with those reported in other studies by Huan et al. [14, 16]. The variation in R_s and ρ of tin oxide with tungsten contribution can be clarified with existence of different valance states of tungsten. As tungsten is added into TO, a part of the Sn^{4+} ions substitute with W^{6+}, and they cause a decrease in R_s and ρ [13–16]. Therefore, a reduction in R_s and ρ is identified with 3 at % W contribution level. In this condition, W behaves as a donor atom. Beyond 3 at % of W contribution level, several of W^{6+} ions fall to the low valance states and this cause to form acceptor states and to lose the number of free carriers. In this way, an increase R_s and ρ is observed. In literature, it has been found that 3 at % and 3 wt % W contribution levels caused a minimum the sheet resistance of TO. In these studies, it was also found that W atoms completely ionized to the valence of 6+, and the best part of W^{6+} entered to the TO structure at little corporation levels from XPS study [13–16]. Also, from theoretical calculations, Zhou et

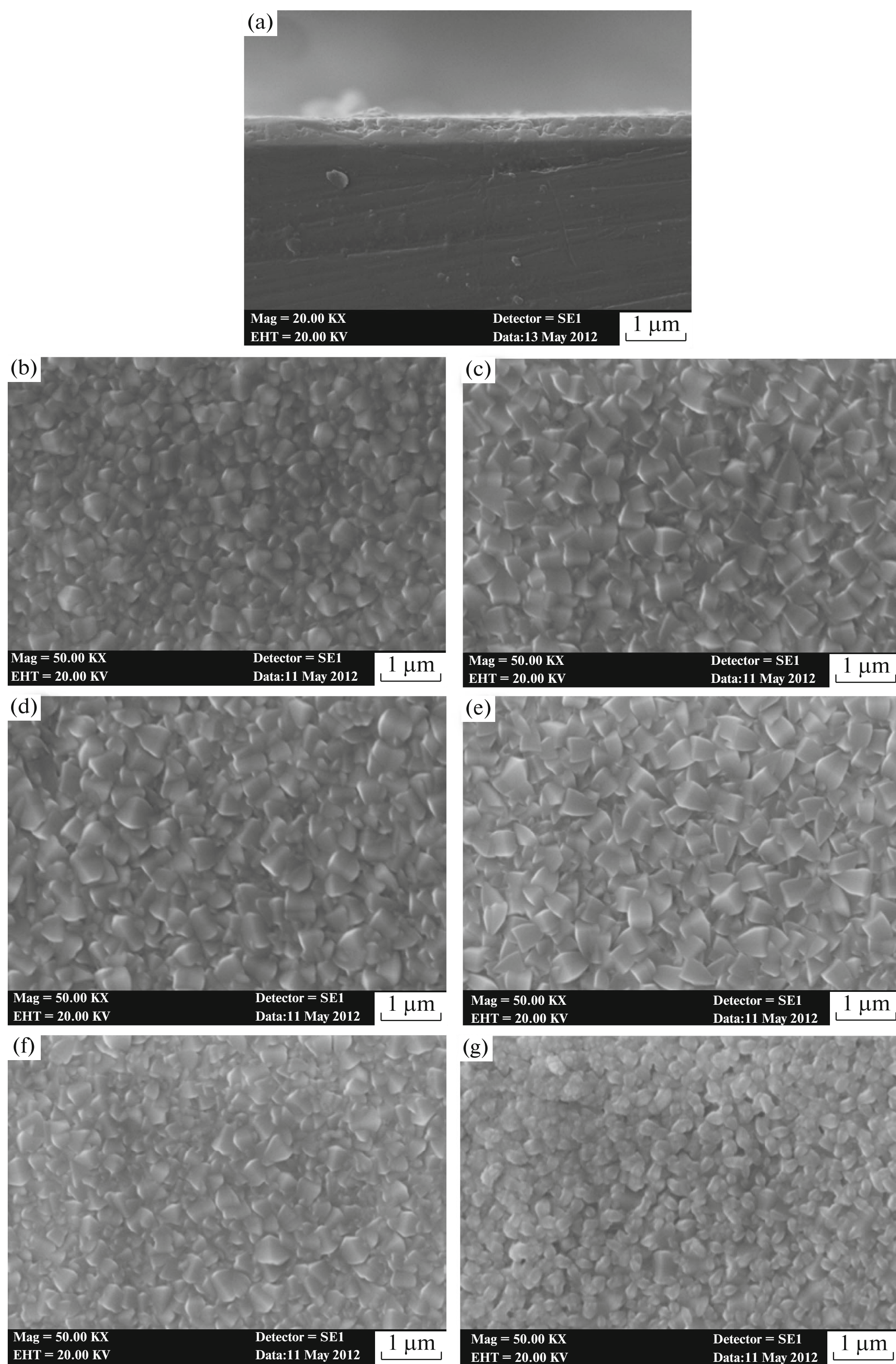

Fig. 4. SEM images of WTO thin films; (a) cross-sectional SEM image, (b) undoped (c) 1 at % W doped (d) 2 at % W doped (e) 3 at % W doped (f) 4 at % W doped (g) 5 at % W doped TO.

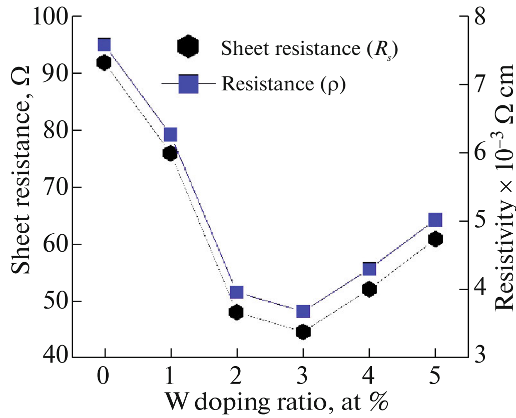

Fig. 5. W doping ratio dependence of sheet resistance and resistivity for sprayed WTO.

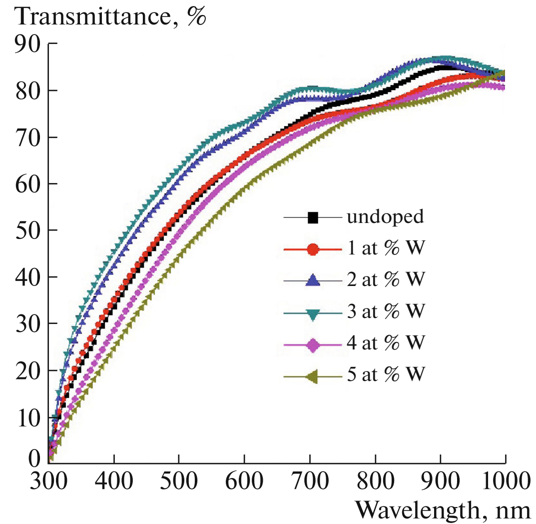

Fig. 6. Optical transmittance spectra of WTO thin films.

al. [32] have found that W doping improved electrical conductivity of TO structure.

3.4. Optical Features

Optical characteristics of samples were inquired by UV-VIS spectrometer at room temperature. Figure 6 reveals the transmittance plots as a function of wavelength for pure and W incorporated TO samples. It can be noticed that the transmission of films is highly influenced with W contribution. It is observed that the transmittance increases with the increasing W contribution up to 3 at % W content and then it decreases with further W contribution level. The absorption coefficient (α) is identified by the equation [20]:

$$\alpha = \ln(1/T)/d \tag{5}$$

The optical band gap (E_g) for WTO samples is assigned by following relation [20]:

$$\alpha h\nu = A(h\nu - E_g)^{1/2} \tag{6}$$

The E_g values are identified by drawing $(\alpha h\nu)^2$ vs. $h\nu$ and extrapolating of the linear region of the plot to zero absorption ($(\alpha h\nu)^2 = 0$).The E_g values for pure, 1, 2, 3, 4 and 5 at % W doped TO thin films are specified as 3.84, 3.87, 3.89, 3.91, 3.79 and 3.71 eV, respectively. It is clearly seen in Fig. 7 that the increasing W content up to 3 at % brings about an increase in the E_g values for TO structure and more W contribution causes a decrease for band gap value of TO. An increment in E_g with W level can be clarified to be following; TO is one of the degenerate transparent oxides [3] and its Fermi level is inside of conduction band [33]. The optical band gap is connected to the excitation of the electrons from the valance band to Fermi level [23, 30]. This implies that an increase in the free carrier concentration resulted from replacing of Sn^{4+} ions with W^{6+} cause a climbing of Fermi level to conduction band and so it is observed optical band gap widening. This phenome is known to be Moss-Burstein effect [34]. A decrease in E_g and transmittance beyond 3 at % of W doping can be due to the enhancement in photon scattering because of crystal defects, impurities, lattice strain created by tungsten doping [35–38].

The figure of merit is a significant parameter to evaluate TCOs [39]. It is determined by Haacke formulation [23];

$$\Phi = T^{10}/R_s \tag{7}$$

where T is the transmittance at 550 nm and R_s is sheet resistance. This formula gives more weight to the transparency and thus is better adapted to solar cell technology. The calculated figure of merit values are

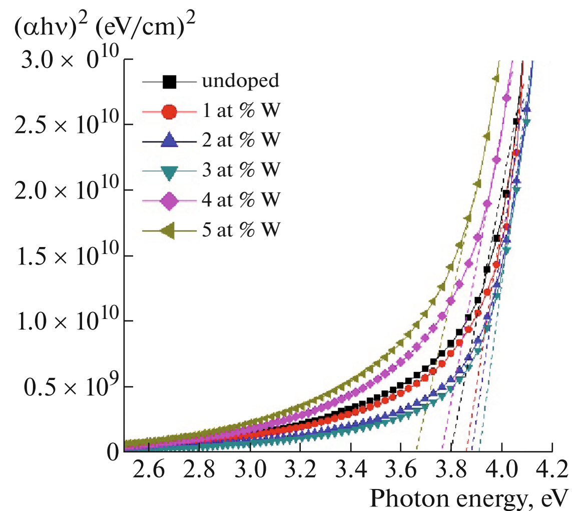

Fig. 7. The variation of $(\alpha h\nu)^2$ vs. $h\nu$ for undoped and WTO thin films.

given in Table 3. It is observed that 3 at % W incorporated films has the maximum value obtained in present study (75.74×10^{-5} Ohm^{-1}). This is possible due to formation of good quality of film in terms of conductivity and transmittance only at this deposition concentration.

As a result, it was deposited pure and W incorporated SnO_2 films for first time by spray pyrolysis technique. However, it is necessary to compare properties of films. For this reason, a comparison of electrical and optical properties of spray deposited W doped SnO_2 films with studies in literature [13–18, 40–42] is made in Table 4. In Table 4, the films deposited by pulsed plasma deposition (PPD) and pulsed laser deposition (PLD) have slightly better electrical and optical characteristics than this study. But, the films grown by sol-gel process and reactive deposition have worse features than present work. This clearly indicates that W doped SnO_2 films fabricated by spray pyrolysis, which is more cheap and simple than PPD and PLD, have great importance for scientific aspect.

4. CONCLUSIONS

This study presents that fabrication and characterization of W doped TO films by spray pyrolysis for the first time. The XRD analysis reveals that the films have polycrystalline tetragonal crystalline property. From XRD and SEM studies, it is seen that the grain size and preferential orientation of the films are affected with W doping concentration. The lowest sheet resistance (44.67 Ohm) and resistivity (3.685×10^{-3} Ohm cm), the highest direct optical band gap (3.91 eV) and figure of merit (75.74×10^{-5} Ohm^{-1}) are obtained for 3 at % W doped films. This work clearly shows that certain features of spray deposited tin oxide depend on W contribution concentration and the WTO films are very well candidates for optoelectronic devices and sensor applications.

REFERENCES

1. E. Elangovan and K. Rammamurthi, Thin Solid Films **476**, 231 (2005).
2. E. Elangovan and K. Ramamurthi, Cryst. Res. Technol. **38**, 779 (2003).
3. M. Batzill and U. Diebold, Progr. Surf. Sci. **79**, 47 (2005).
4. A. V. Moholkar, S. M. Pawar, K. Y. Rajpure, P. S. Patil, and C. H. Bhosale, J. Phys. Chem. Solids **68**, 1981 (2007).
5. G. Turgut, E. Sonmez, S. Aydin, R. Dilber, and U. Turgut, Ceram. Int. **40**, 12891 (2014).
6. K. Ravichandran, G. Muruganantham, and B. Sakthivel, Physica B: Condens. Matt. **404**, 4299 (2009).
7. G. Jain and R. Kumar, Opt. Mater. **26**, 27 (2004).
8. R. R. Kasar, N. G. Deshpande, Y. G. Gudage, J. C. Vyas, and R. Sharma, Physica B: Condens. Matt. **403**, 3724 (2008).
9. E. Elangovan, S. A. Shivahankar, and K. Ramamurthi, J. Crystal Growth **276**, 215 (2005).
10. K. S. Kim, S. Y. Yoon, W. J. Lee, and K. H. Kim, Surf. Coating Technol. **138**, 229 (2001).
11. S. Chacko, N. S. Philip, K. G. Gophandran, P. Koshy, and V. K. Vaidyan, Appl. Surf. Sci. **254**, 2179 (2008).
12. E. Elangovan, M. P. Singh, and K. Ramamurthi, Mater. Sci. Eng. B **113**, 143 (2004).
13. Y. Huang, Q. Zhan, and G. Li, Semicond. Sci. Technol. **24**, 015003 (2009).
14. Y. Huang, D. Li, J. Feng, G. Li, and Q. Zhang, J. Sol-Gel Sci. Technol. **54**, 276 (2010).
15. Y. Huang, G. Li, J. Feng, and Q. Zhang, Thin Solid Films **518**, 1892 (2010).
16. Y. Huang, Q. Zhang, G. Li, and M. Yang, Mater. Character. **60**, 415 (2009).
17. S. Nakao, N. Yamada, T. Hitosugi, Y. Hirose, T. Shimada, and T. Hasegawa, Phys. Status Solidi © **8**, 543 (2011).
18. S. Muranaka and Y. Bando, Bull. Inst. Chem. Res. **70**, 430 (1992).
19. E. Elangovan, M. P. Singh, M. S. Dharmaprakash, and K. Ramamurthi, J. Optoelectr. Adv. Mater. **6**, 197 (2004).
20. T. Serin, N. Serin, S. Karadenzi, H. Sari, N. Tugluoglu, and O. Pakma, J. Non–Crystal. Solids **352**, 209 (2006).
21. A. V. Moholkar, S. M. Pawar, K. Y. Rajpure, and C. H. Bhosale, Mater. Lett. **61**, 3030 (2007).
22. A. V. Moholkar, S. M. Pawar, K. Y. Rajpure, N. Saleh, PatilP. S. Almari, and C. H. Bhosale, Solar Ener. Mater. Solar Cells **92**, 1439 (2008).
23. A. R. Babar, S. S. Shinde, A. V. Moholkar, C. H. Bhosale, J. H. Kim, and K. Y. Rajpure, J. Alloys Comp. 505, 416 (2010).
24. A. Smith, D. S. Laurent, D. S. Smith, J. P. Bonnet, and R. R. Clemente, Thin Solid Films **226**, 20 (1995).
25. G. C. Morris and A. E. McElnea, Appl. Surf. Sci. **92**, 167 (1996).
26. S. Chacko, N. S. Philip, K. G. Gophandran, P. Koshy, and V. K. Vaidyan, Appl. Surf. Sci. **254**, 2179 (2008).
27. G. Turgut, E. F. Keskenler, S. Aydin, M. Yilmaz, S. Dogan, and B. Duzgun, Phys. Scripta **87**, 035602 (2013).
28. M. Dhanam, P. K. Manoj, R. Rajeev, and R. Prabhu, J. Cryst. Growth **280**, 425 (2005).
29. A. R. Babar, S. S. Shinde, A. V. Moholkar, C. H. Bhosale, J. H. Kim, and K. Y. Rajpure, J. Semicond. 32, 053001 (2011).
30. A. R. Babar, S. S. Shinde, A. V. Moholkar, C. H. Bhosale, J. H. Kim, and K. Y. Rajpure, J. Alloys Compd. **509**, 3108 (2011).
31. K. Ravichandran and P. Philominathan, Mater. Lett. **62**, 2980 (2008).
32. W. Zhou, L. Liu, M. Yuan, Q. Song, and P. Wu, Compt. Mater. Sci. **54**, 109 (2012).
33. J. J. Lingane and L. A. Small, J. Am. Chem. Soc. **71**, 973 (1949).
34. E. Burstein, Phys. Rev. **93**, 632 (1954).
35. F. Yakuphanoglu, Y. Caglar, S. Ilican, and M. Caglar, Physica B: Condens. Matt. **394**, 86 (2007).

36. G. Turgut and E. Sonmez, Metall. Mater. Trans. A **45**, 3675 (2014).
37. L. B. Fewuns and S. Suresh, *Thin Film Materials: Stress, Defect Formation and Surface Evolution* (University Press, Cambridge, 2003).
38. G. Turgut and E. Sonmez, Superlatt. Microstruct. **69**, 175 (2014).
39. G. Turgut, E. F. Keskenler, E. Sonmez, S. Dogan, B. Duzgun, and M. Ertugrul, Superlatt. Microstruct. **56**, 107 (2013).
40. E. F. Keskenler, G. Turgut, S. Aydin, and S. Dogan, Optik **124**, 4827 (2013).
41. A. Kurz, K. Brakecha, J. Puetz, and M. A. Aegerter, Thin Solid Films **502**, 212 (2006).
42. G. Turgut, E. F. Keskenler, S. Aydin, D. Tatar, E. Sonmez, S. Dogan, and B. Duzgun, Rare Met. **33**, 433 (2014).